CHAPTER 3

Design of an experimental vibration absorber

3.1 Introduction

This chapter will document the proposed design methodology for a LIVE type vibration absorber. The main objective of the absorber is to isolate at the excitation frequency. Equation 2.63 shows that the isolation frequency is a function of many variables and several sets of these will isolate at the design frequency. Some sets will give better isolation than others will, and this can be used to reduce the number of possible solutions. Even after this criterion has been satisfied several possible solutions still exist. The particular application will also have additional specific demands regarding size, weight, static deflection and others, which will be used to choose the optimal solution.

Two design methods will be discussed. The first is an iterative design approach, which is rather tedious, but this method will be used to explain the design process and will give some insight into the problem. The second method uses constrained optimisation. This method is more efficient and can be used to do several designs in order to study the effect each variable has on the transmissibility and isolation frequency.

Using these methods an experimental absorber was designed. This absorber was manufactured and extensively tested to verify this design methodology as well as to get practical experience with some of the manufacturing and design difficulties. The design difficulties mainly originated from the requirement that the port must be able to move axially in a cylinder with closed ends. This necessitated connection through the side of the outer cylinder, which proved difficult to manufacture.

Two important aspects of the design are the spring rate of the elastomeric spring and the damping caused by the liquid. The available methods to estimate the spring's stiffness will be discussed. The damping constant was calculated using computational fluid dynamics and the result will be reported.

The chapter will start with the final design showing its parts and explaining the variables that will influence its performance.

3.2 The experimental absorber

This paragraph will highlight some of the practical aspects of the absorber's design. It will introduce the parts and list their requirements. It will also show which dimensions will influence its performance. Finally the choice of absorber liquid will be justified.

3.2.1 Absorber parts

The absorber consists of a port that can move axially relative to a concentric cylinder (sleeve). The port is connected to the sleeve with a polyurethane spring, which is cast in this position and is rigidly fixed to the port and the sleeve. To facilitate the axial movement the port and the sleeve must be connected to the opposite ends of the absorber. The port is connected via a connector block, connector cylinder and lid to the top load cell. The sleeve is connected using the bottom plug. The plugs form reservoirs of fluid that will be accelerated through the port when relative axial movement between the port and sleeve occurs. Additional detail relating to the design can be found in appendix F.

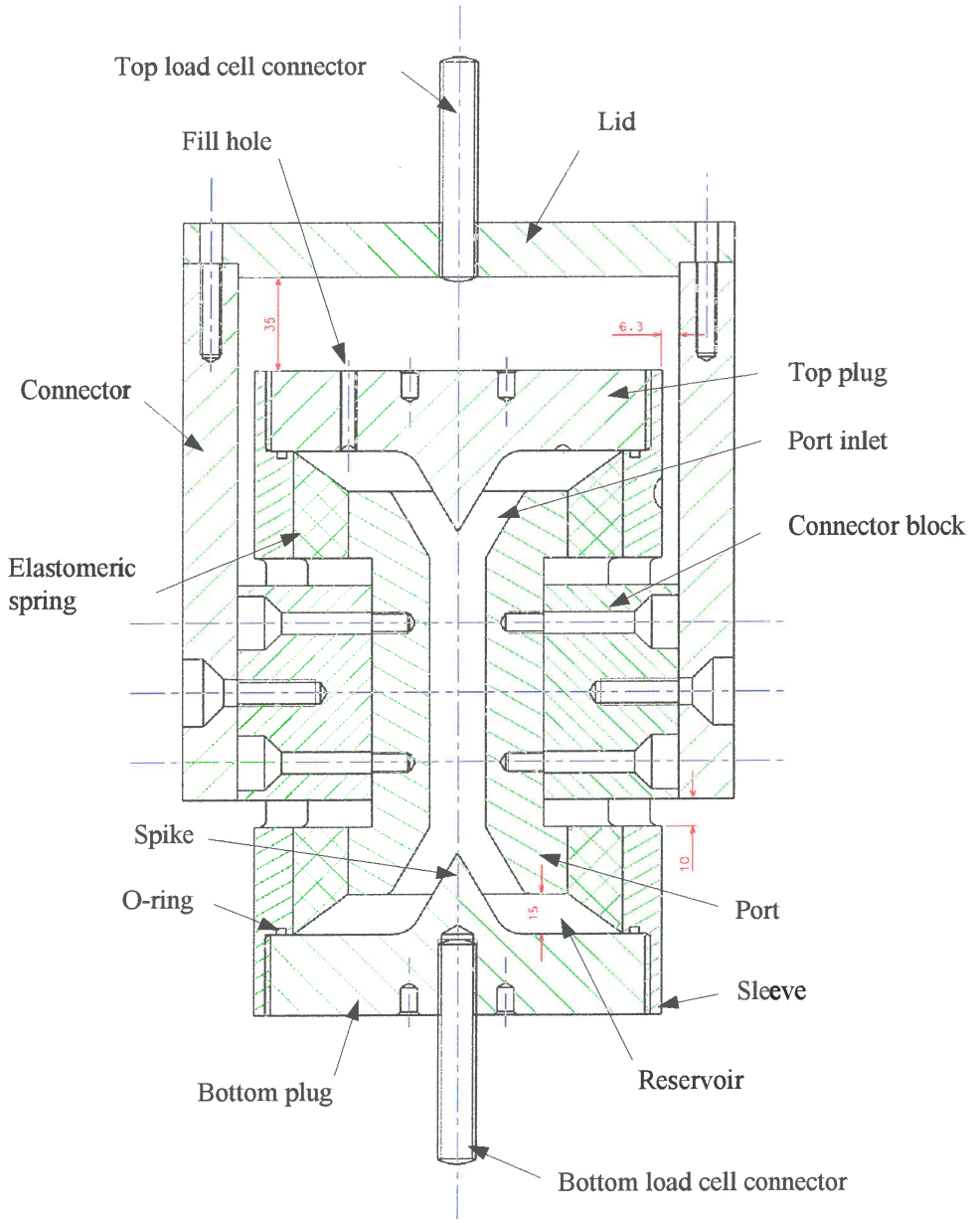

Figure 3.1 Absorber assembly showing clearances and parts

The connection of the port with the top load cell was the most difficult part of the design. The purpose of the connection is to transfer the force from the actuator at the bottom to the fixed load cell at the top. The connection had to:

- transfer a buckling moment from the actuator to the load cell,
- be free from play in the axial direction, and
- have high axial stiffness compared to the elastomeric spring so as not to have an influence on the absorbers performance.

The connector blocks transfer the buckling moment from the connector to the port. These blocks were curved on their outer side and thus could not rotate in the connector, which had the same curvature. The block was fitted to the connector using a M16 flat head socket screw and was fixed to the port using two M8 flat head socket screws. This was done to prevent rotation as the interface between the block and the port is flat. The lid was fitted to the connector using 6 M8 allencap screws. The lid was fixed to the load cell with a M14×2 threaded rod. It is of extreme importance that there should be no free play in the axial direction since this will have a negative impact on the absorber's performance. The play was minimised by using two sets of screws to fit the connector to the port via the connector block. Flat head socket screws were used to ensure a tight fit on the seat surface.

The absorber was designed for a maximum of 10 mm axial displacement, which is more than would be needed but will make it possible to fit very soft springs in future tests. The 6.3 mm gap between the connector and the sleeve should accommodate any radial misalignment between the two load cell connection points.

In the top plug a M6 fill hole was used to add the absorber fluid. At the bottom of this plug a groove was machined to facilitate the escape of air from inside the reservoir. It is important that there should be no trapped air in the reservoir because this will negate the all-important conservation of mass between the reservoir and the port. Both the plugs were fitted with 6 mm holes which were used to tighten the plug on the 3 mm O-ring.

3.2.2 Design variables

The basic design variables are shown in figure 3.2. Decisions made about each of these will influence the absorber performance. The required isolation frequency and transmissibility determined the values of some of these variables. The size of the side entrances is influenced by the clearance required between the connector block and the sleeve as well as the size of the screws used, the distance required between them to transfer the moment and the size of the curved surface on the outer side. The size of the side entrance, the port outer diameter and

the reservoir height will in turn influence the spring stiffness. The dimensions of the spike, and the inlet entrance will influence the viscous damping.

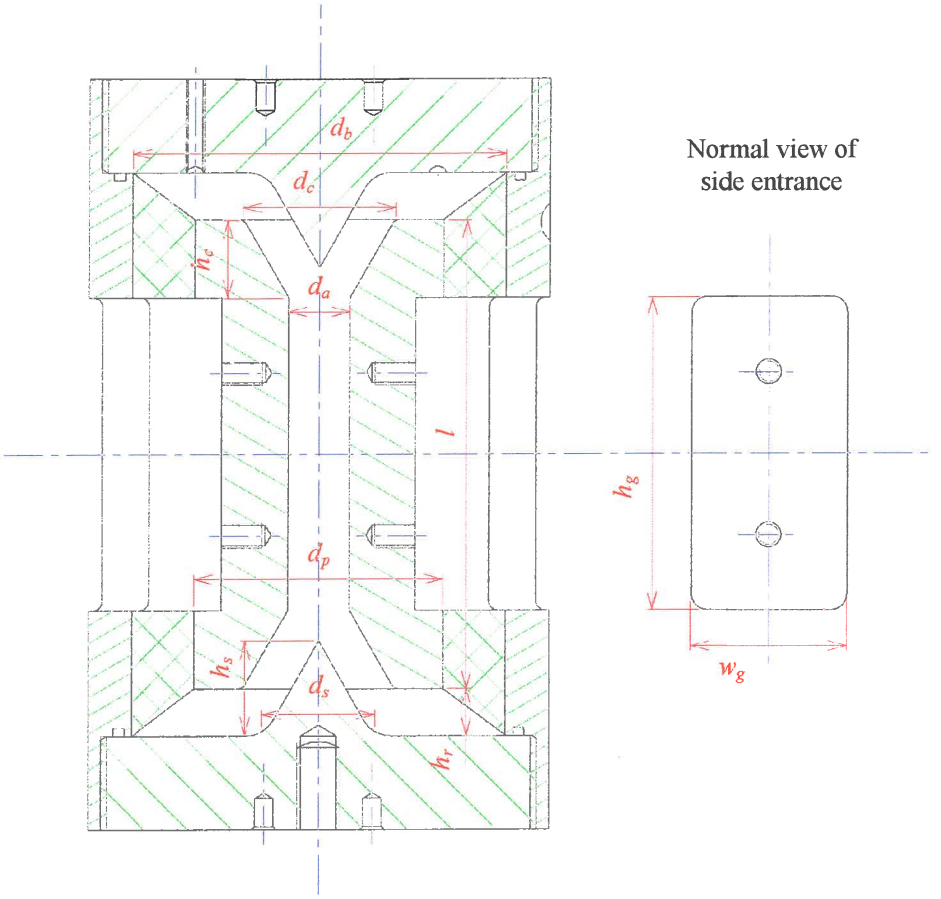

Figure 3.2 Basic design variables

Table 3.1 Basic design variables

Variable	
Port length	l
Port inner diameter	d_a
Port outer diameter	d_p
Reservoir diameter	d_b
Inlet height	h_c
Inlet entrance diameter	d_c
Spike height	h_s
Spike base diameter	d_s
Reservoir height	h_r
Gap height	h_g
Gap width	w_g

3.2.3 Absorber liquid

This absorber was designed to use water as the absorber liquid. Halwes (1980) stated that the absorber size will be inversely proportional to the square of the density of the absorber liquid. High-density liquids will therefore result in smaller absorbers. If this design was done using mercury the reservoir diameter would have been less than half of the absorber using water. The following properties are however required of the absorber liquid:

- High density
- Low-toxicity
- Liquid at expected working temperature (-10 to 50 °C)
- Low viscosity (low damping)
- Non-corrosive (elastomers, steel)
- Non-abrasive (elastomers, steel)
- Inexpensive
- Available

Table 3.2 Summary of liquid properties at 25°C

Liquid		ρ [kg/m^3]	μ [N.s/m^2]	T_m [°C]	T_b [°C]	Hazard rating*
Water	H_2O	998	1.00×10^{-3}	0	100	0
Bromine	Br_2	3113	0.91×10^{-3}	-7	59	4
Bromoform	$CHBr_3$	2894		N/A	150	3
Carbon tetrachloride	CCl_4	1590	0.97×10^{-3}	-23	76	3
Lead tetrachloride	$PbCl_4$	3174		-15	105	
LST		2954				
Mercury	Hg	13550	1.56×10^{-3}	-38	356	4
Phosphorous tribromide	PBr_3	2846		-40	173	3
Selenium bromide	Se_2Br_2	3597			227	
Selenium monochloride	Se_2Cl_2	2764		-85	130	
Tetrabromoacetylene	$Br_2CHCHBr_2$	2954		0	135	2
Thionyl bromide	$SOBr_2$	2675		-52	138	
Thiophosphorylbromidechloride	$PSBr_2Cl$	2475		-60	95	
Tindibromidedichloride	$SnBr_2Cl_2$	2814		-20	65	

* Baker SAF-T-DATA™ health rating, 0 = no hazard, 4 = extreme hazard.

Most heavy liquids are too hazardous to consider as possible absorber fluids. The only liquid that will have a significant impact on absorber size is mercury. However, the benefit of using mercury will be offset by the cost involved in ensuring that it doesn't find its way into the environment. Mercury will also result in higher damping than water because the turbulent shear stress is a function of density and viscosity. Water with a corrosion inhibitor additive is recommended for a screen where the size of the absorber is not as critical.

3.3 Design methodology

The isolation frequency is the most important quantity in the design process. In chapter 2 the tuning equation was derived giving the relationship between the five variables and the isolation frequency. The simplified equation is:

$$\omega_a = \sqrt{\frac{k}{\rho l\left(\frac{A_b}{A_a}-1\right)A_b}} \tag{3.1}$$

At first glance it appears obvious to simply choose four of the variables and calculate the remaining one using equation 3.1. However, this approach neglects the effect that the choice of parameters will have on a damped system's transmissibility and the absorber's size. The transmissibility can be written in terms of the five variables as follows (from equation 2.61):

$$\frac{F_o}{F_i} = \frac{k(1+i\eta)+i\omega c+\omega^2\rho l\left(1-\frac{A_b}{A_a}\right)A_b}{k(1+i\eta)+i\omega c-\omega^2\left[m+\rho l A_a\left(1-\frac{A_b}{A_a}\right)^2\right]} \tag{3.2}$$

It can be assumed that a set of optimal parameters exist that will minimise the transmissibility at the frequency of isolation while also satisfying certain size constraints. It seems therefore that the design of the absorber lends itself to an optimisation approach. However, it was found that the optimisation design method does not lead to significant insight. To address this shortcoming an iterative design method will be discussed first. This design will be done for an application with an operating frequency of 50 Hz. Although this is not a common screen operating frequency it will be sufficient for the validation of the mathematical model. It will also simplify the design and can be accommodated by the available hydraulic actuator.

3.3.1 Iterative design approach

As noted before, the specific application will fix the isolation frequency and thus by choosing any four parameters the remaining one can be calculated using equation 3.1. The analysis can be simplified by reducing the number of variables available for tuning from five to two, which is achieved by introducing the absorber mass into equation 3.1:

$$m_B = \rho l A_a \tag{3.3}$$

The absorber mass is written as a function of area ratio, isolation frequency and stiffness:

$$m_B = \frac{k}{\omega_a^2\left(\frac{A_b}{A_a}-1\right)\frac{A_b}{A_a}} \tag{3.4}$$

A second criterion must also be satisfied namely low transmissibility. The transmissibility is written in non-dimensional form so as to simplify accounting for the effect of damping:

$$|T_r| = \left\{ \frac{\left[1-\left(\frac{\omega}{\omega_a}\right)^2\right]^2 + \left[2\zeta\frac{\omega}{\omega_n}+\eta\right]^2}{\left[1-\left(\frac{\omega}{\omega_n}\right)^2\right]^2 + \left[2\zeta\frac{\omega}{\omega_n}+\eta\right]^2} \right\}^{\frac{1}{2}} \tag{3.5}$$

From the analysis in chapter 2 we know that the natural frequency must be small compared to the isolation frequency. Figure 3.3 reiterates this by showing a region of low transmissibility for a system with low stiffness. Another important feature of the figure is the infeasible design region below the red area. In this area the natural frequency is higher than the isolation frequency resulting in high frequency amplification.

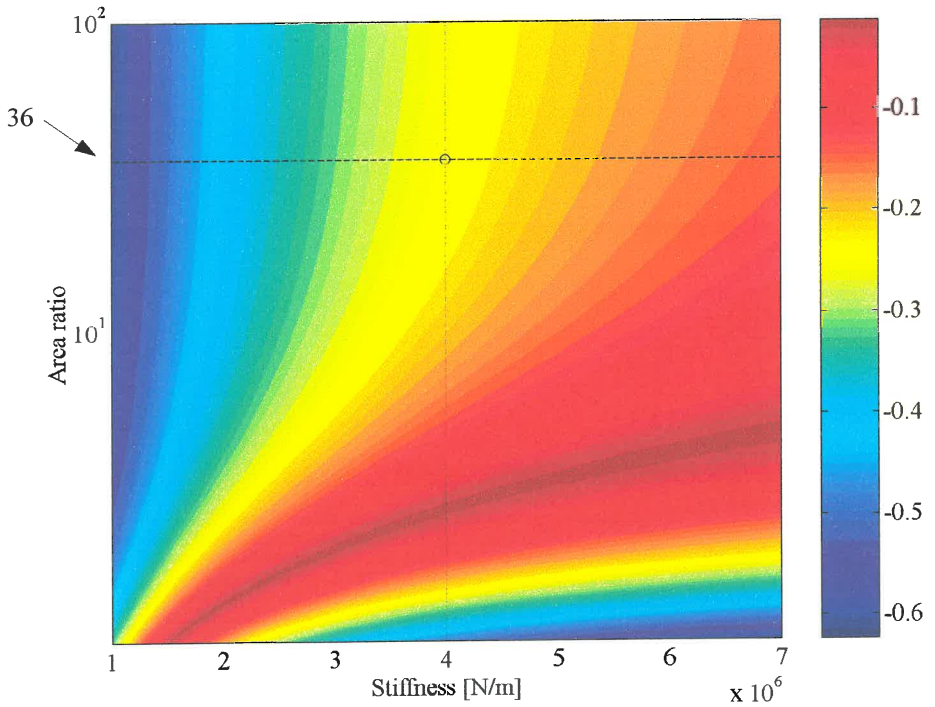

Figure 3.3 The min(log$|T_r|$) as a function of area ratio and stiffness for $f_a = 50$ Hz and with $m = 15$ kg, $\rho = 1000$ kg/m^3, $\eta = 0.1$ and $\zeta = 0.1$

From figure 3.3 it is clear that a high area ratio and low stiffness will minimise the transmissibility. There are, however, constraints on the area ratio and the stiffness. Most practical applications can only accommodate a certain amount of static deflection. This deflection will therefore be the lower bound of the stiffness. The elastomeric material properties and the space available for installation also influence the stiffness. Polyurethane was chosen as the preferred material because of its low loss factor and ease of manufacture.

Although the polyurethane was available in hardnesses ranging from 35 to 90 Shore A, they all will result in a rather stiff spring. After some calculations were done regarding the available shear modulus of elasticity and some reasonable geometries, 4 MN/m was chosen as the design stiffness. This choice fixed the vertical stiffness line as shown on figure 3.3.

Furthermore a high area ratio will result in either a small port diameter or a large reservoir diameter. The port diameter is constrained by the viscous damping. Equation 2.28 shows that the damping is a function of port diameter. High area ratios will also increase the inlet and outlet losses as well as the port velocity. The port reservoir diameter was chosen as 120 mm which makes the absorber bulky but manageable. Figure 3.3 shows that the gain in transmissibility decreases rapidly at high area ratios. For this reason as well as the increase in damping the area ratio was fixed at 36.

The length of the port is constrained by the buckling moment that needs to be transferred across the absorber when it is in compression.

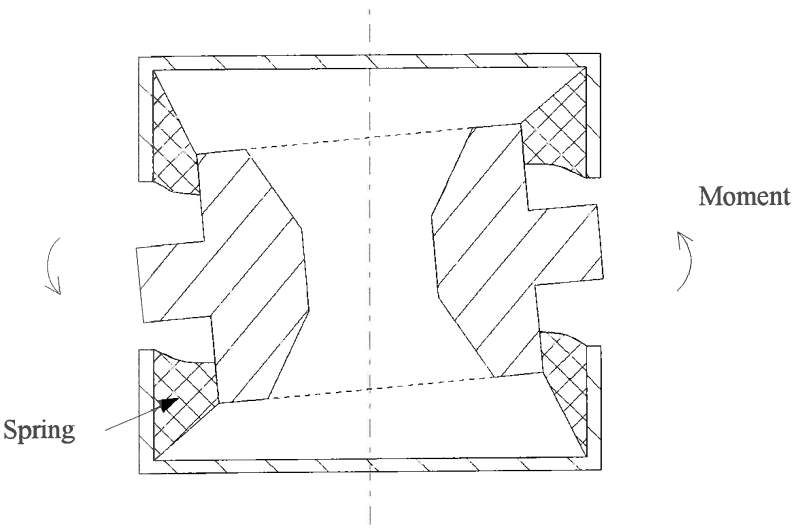

Figure 3.4 Schematic explanation of the necessity to transfer the buckling moment

To transfer the buckling moment a certain thickness, length and modulus of elasticity is required of the elastomeric spring. The thickness is governed by the outer diameter of the port since the reservoir diameter is fixed by the overall size constraint. This diameter is also influenced by the required axial stiffness of the spring as well as the attachment method. A reasonable design approach would be to specify a minimum ratio of port length to port inner diameter. This will leave the rather complex specification of a port outer diameter to be determined by the required axial stiffness. The following slenderness ratio was recommended:

$$\frac{l}{d_a} \geq 6 \qquad \textbf{(3.6)}$$

The only other property that will influence the design is the density of the absorber liquid. From the above analysis it is clear that the size of the absorber will be influenced significantly by the density. If the density is increased the area ratio can be decreased which will result in a smaller absorber. The variables discussed above are summarised in the following table.

Table 3.3 Design variables

Design variable		Value
Stiffness [MN/m]	k	4
Area ratio	A_r	36
Undamped isolation frequency [Hz]	f_a	50
Reservoir diameter [mm]	d_b	120
Density [kg/m^3]	ρ	1000

Using these design variables the remaining unknowns in equation 3.1 can be calculated.

Table 3.4 Design results

Unknowns	From		Value
Port diameter [mm]	From area ratio	d_a	20
Absorber mass [kg]	From tuning equation 3.4	m_B	4.02×10^{-2}
Volume [m^3]	From absorber mass and equation 3.3	$\frac{\pi}{4}d_a^2 l_{\min}$	4.02×10^{-5}
Port length [mm]	Port volume	l_{min}	102
Slenderness ratio	Test in length conforms to equation 3.6	l_{min}/d_a	6.4

The designer must also take into account the shift that occurs in the isolation frequency due to damping. Assuming that the design will have a loss factor and a viscous damping ratio both of 0.1, the transmissibility curve can be calculated. From this curve the final results for the absorber's physical properties can be found and these are shown in table 3.5.

Table 3.5 Designed absorber's physical properties $\zeta = 0.1$, $\eta = 0.1$

Property	Design	Minimum
Transmissibility	0.70	0.57
Isolation frequency [Hz]	50	56.96

It is important to note that since the port length was calculated using the undamped isolation frequency of 50 Hz, the damped minimum only occurred at 56.96 Hz. This resulted in a less than optimal design as can be seen from figure 3.5. However, the length calculated in this way is useful since it represents a minimum port length. A simple search for the minimum

transmissibility can now be done by increasing the port length, starting at the calculated minimum value. This is shown in figure 3.6.

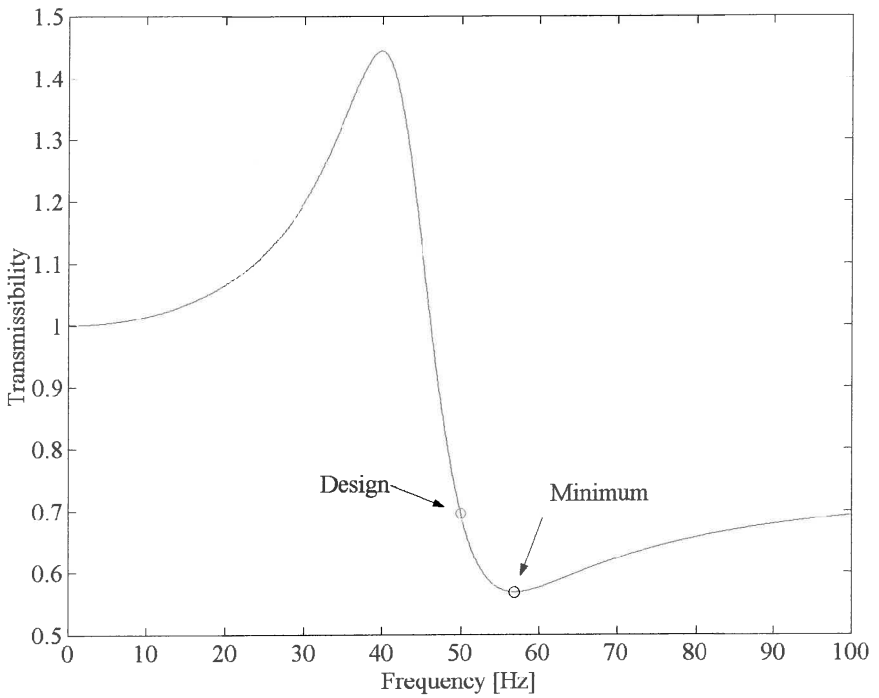

Figure 3.5 Minimum transmissibility search with $m = 15$ kg, $\zeta = 0.1$ and $\eta = 0.1$

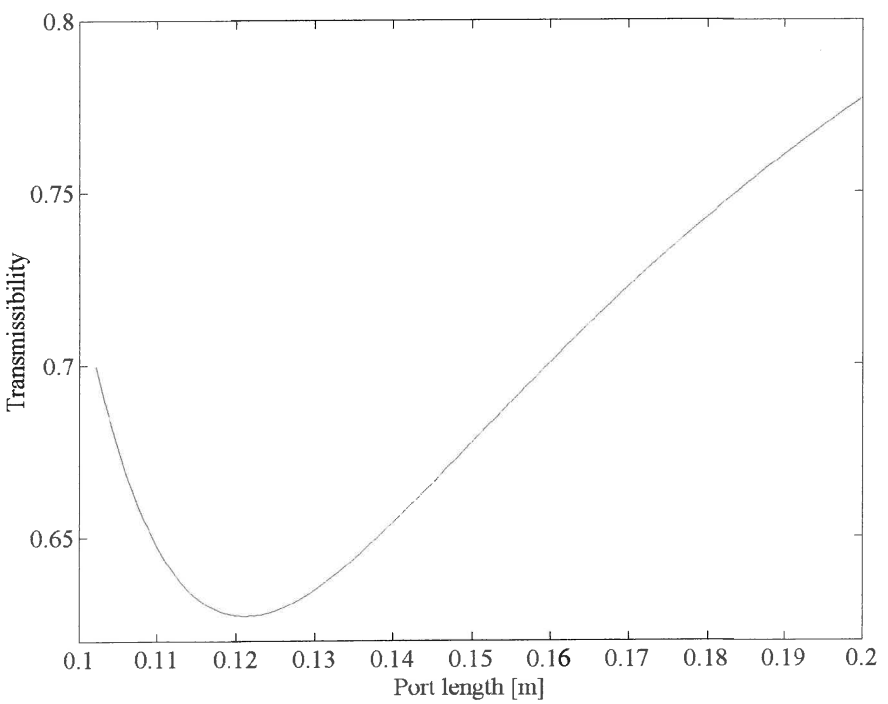

Figure 3.6 Minimum transmissibility search with $m = 15$ kg, $\zeta = 0.1$ and $\eta = 0.1$

This procedure resulted in the transmissibility plot shown in figure 3.7. The original design is shown in blue and the new design in green. The isolation frequency cannot be decreased without increasing the transmissibility.

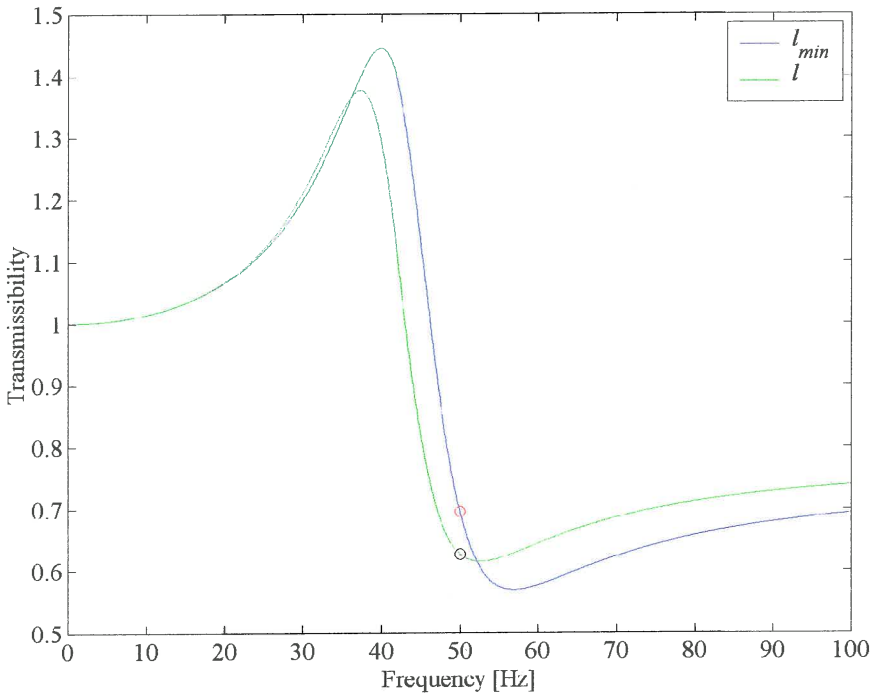

Figure 3.7 Ideal transmissibility for isolation at 50 Hz (green) and the transmissibility curve of the design done using the undamped isolation frequency (blue) with $m = 15$ kg, $\zeta = 0.1$ and $\eta = 0.1$

The optimal port length was 121 mm and the transmissibility for this design 0.63, which is significantly better than the first design. It is important to note that the minimum on this curve is not the optimal transmissibility either. This design will be sensitive to changes in excitation frequency and it could therefore be beneficial to sacrifice transmissibility for bandwidth by lengthening the port further.

The addition of the conical port inlet/outlet must still be taken into account. The effect of the addition is to increase the isolation frequency. Increasing the port length will counteract this increase. The isolation frequency ratio given by equation 2.75 will be used to calculate the port length, which will result in the same isolation frequency as an absorber with a square inlet/outlet. The required ratio between the isolation frequency of a port with and without an absorber is 1 and the equation can therefore be re-written as follows:

$$l' = l + 2h_c - 2\frac{A_a}{A_c}\left(\frac{h_p^2}{h_p - h_c} - h_p\right) \tag{3.7}$$

The inlet geometry and its effect on the port length are summarised in Table 3.6.

Table 3.6 Port length adjustment

Design variable [mm]		Value
Original port length	l	121.0
Inlet height	h_c	25.0
Inlet entrance diameter	d_c	48.9
Port diameter	d_a	20.0
Port cone height	h_p	42.3
Adjusted port length	l'	150.5

The lengthening of the port will result in slightly higher viscous damping.

At the beginning of the design it was assumed that a 4 MN/m spring could be moulded in the available space. This should now be verified using the approach that will be discussed later in §3.4. If these calculations prove that it is impossible to achieve the desired stiffness the design must be attempted using the same procedure with a new stiffness.

3.3.2 Optimisation approach

Using optimisation to solve this problem simplifies the design process. Given a set of constraints the transmissibility is minimised at a specific frequency. The results are exactly the same as in the previous section, but the process is more efficient, especially if several designs are needed.

The variables are listed table 3.7.

Table 3.7 Variables and constraints

Design variable		Optimisation variable	Bound
Stiffness [MN/m]	k	x_1	≥ 4
Reservoir diameter [mm]	d_b	x_2	≤ 120
Port diameter [mm]	d_a	x_3	≥ 20

All the variables are of course physical properties and cannot be less than zero.

The objective function and the constraints are:

$$f(\bar{x}) = \left| \frac{x_1(1+i\eta)+i\omega_a 2\zeta\sqrt{x_1\left[m+\frac{\pi}{4}\rho x_4 x_2^2\left(1-\frac{x_3^2}{x_2^2}\right)^2\right]}+\frac{\pi}{4}\omega_a^2\rho x_4 x_3^2\left(1-\frac{x_3^2}{x_2^2}\right)}{x_1(1+i\eta)+i\omega_a 2\zeta\sqrt{x_1\left[m+\frac{\pi}{4}\rho x_4 x_2^2\left(1-\frac{x_3^2}{x_2^2}\right)^2\right]}-\omega_a^2\left[m+\frac{\pi}{4}\rho x_4 x_2^2\left(1-\frac{x_3^2}{x_2^2}\right)^2\right]} \right|$$

subject to

(3.8)

$$g_1(\bar{x}) = -x_1 + k^{\min} \le 0$$
$$g_2(\bar{x}) = x_2 - d_b^{\max} \le 0$$
$$g_3(\bar{x}) = -x_3 + d_a^{\min} \le 0$$
$$g_4(\bar{x}) = \sqrt{\frac{x_1}{m+\frac{\pi}{4}\rho x_4 x_2^2\left(1-\frac{x_3^2}{x_2^2}\right)^2}} - \omega_a \le 0$$

The objective function was found by substituting the viscous damping in terms of the damping ratio and critical damping. The first three constraints are the same as were discussed in §3.3.1. The last constraint ensures that the design is in the feasible region where the natural frequency is smaller that the design isolation frequency. Without this constraint the solution can get stuck at a local minimum which is larger than the global minimum.

Table 3.8 Optimisation variables

Design variable		Optimisation variable	Optimum
Stiffness [MN/m]	k	x_1	4
Reservoir diameter [mm]	d_b	x_2	120
Port diameter [mm]	d_a	x_3	20
Port length [mm]	l	x_4	121

The MATLAB constrained optimisation algorithm `fmincon.m` was used for the optimisation. At the optimum design point the stiffness was at the minimum and the area ratio at the maximum allowed by the constraints. This confirms the previous analysis. The resulting transmissibility plot is the same as shown in figure 3.7. The problem must not be over-constrained by adding a maximum bound on the port length. This constraint will not allow the algorithm to find the minimum. Equation 3.7 can now be used to calculate the port length that will offset the port inlet/outlet geometry.

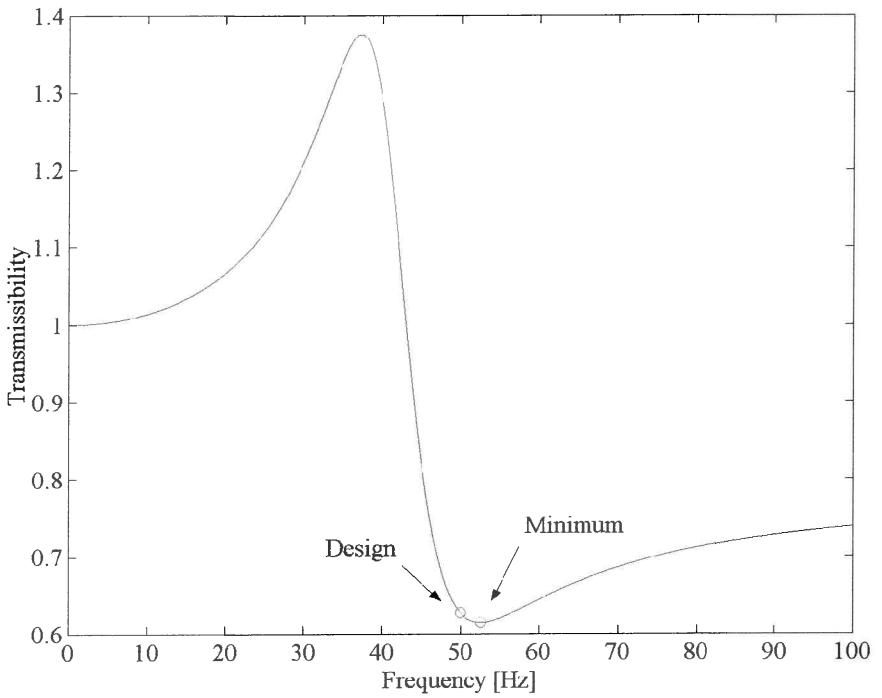

Figure 3.8. Ideal transmissibility curve for isolation at 50 Hz with $m = 15$ kg, $\zeta = 0.1$ and $\eta = 0.1$

If it is deemed that it will be more beneficial to locate the minimum transmissibility to coincide with the isolation frequency the approach suggested in chapter §2.7.2 can be used. The absolute value of the transmissibility was differentiated to give an expression for the curve's minimum and maximum frequency. It was found that the minimum corresponds to the second root of a rather complex polynomial. This equation cannot be solved analytically and a numerical search procedure had to be used. The MATLAB function `fsolve.m` was used to minimise the absolute value of the difference between the second root and the isolation frequency. This function uses a least-squares method to find the optimal length that will minimise the objective function. This procedure resulted in a design with a slightly longer port length and higher transmissibility than was found previously. The results are summarised in table 3.9.

Table 3.9 Port length and transmissibility

Search result		Value
Port length [mm]	l	135
Transmissibility	$\lvert T_r \rvert$	0.64

This port length can also be adjusted so that the inlet/outlet geometry can be taken into account using equation 3.7.

3.4 Calculation of the spring stiffness

The stiffness is a function of the material and the geometry. The material properties will be discussed first. In the following paragraphs the geometry will be analysed through successive refinements. The spring will first be estimated as a hollow cylinder, then as a cylinder with tapered ends and lastly the effect of the side entrances will be taken into account.

3.4.1 Material properties

Polyurethane will behave non-linearly at large strains. This behaviour is called hyperelasticity. In order to decide if non-linear behaviour is present, the normal strain must be calculated. The shear and normal strains are given by equation 3.9 and 3.10 (Gere & Tomoshenko, 1991):

$$\gamma = \text{atan}\left(\frac{x}{t}\right) \tag{3.9}$$

$$\varepsilon^2 + 2\varepsilon - \sin\gamma = 0 \tag{3.10}$$

Where x is the deflection and t the thickness of the rubber. The following table summarises the shear strain results for a 20 mm thick spring.

Table 3.10 Summary of strain for different deflections

Description	Deflection [mm]	Shear strain	Normal strain
Normal operating	1	0.050	0.0247
Operating maximum	5	0.245	0.1147
Design maximum	10	0.460	0.2030

The static properties of 55-Shore A polyurethane are published by the manufacturer at the three strains shown in table 3.11.

Table 3.11 Published modulus of elasticity vs strain

Modulus of elasticity [MPa]	Strain
1.4	1
3.4	5
6.9	10

The modulus of elasticity at a strain of 0.05 caused by a deflection of 1 mm is estimated as 0.975 MPa. The shear modulus is related to the modulus of elasticity:

$$G = \frac{E}{2(1+\nu)} \tag{3.11}$$

The Poisson's ratio for incompressible materials is 0.5 and the shear modulus is consequently one third of the modulus of elasticity.

The dynamic properties of polyurethane are described by the complex modulus of elasticity as shown in equation 2.44. There are several factors that can influence the dynamic properties relating to the material, load etc. (Garibaldi & Onah, 1996). The most important are the following:

- Temperature. This is the most important factor.
- Frequency. The modulus of elasticity will increase with frequency.
- Strain. If the strains are large the material behaviour is non-linear and the complex modulus will represent an average value.

The value of the complex dynamic modulus of elasticity is not published by the manufacturer and was obtained from tests done at the University of Pretoria. E^* and η was measured as a function of frequency only.

These tests were done with a 40 mm cube that was bonded on two opposite ends. The correct relation between modulus of elasticity and shear modulus for this configuration is given by equation 3.12 (Nashif *et al.*, 1985):

$$E_c = 3G\kappa_T \tag{3.12}$$

$$\kappa_T = 1 + \beta\left(\frac{S}{S'}\right)^2 \tag{3.13}$$

κ_T is known as the shape factor. β is a non-dimensional constant equal to 2 for an unfilled and 1.5 for a filled elastomer. Filler is added to natural rubber to change its properties. Since this is not applicable to polyurethane both values were tested and the shape factor proved to be insensitive to this parameter. S is the cross sectional area (40×40) and S' (40×40×4) the nonload-carrying area. The relation between E and G is therefore slightly less than suggested by equation 3.11. For all the calculations involving data from these tests it will be assumed that the relation is 0.3.

Measurements were done using a 60 Shore A specimen up to an excitation of 30 Hz, at room temperature and at various strains. From these measurements it is estimated that the storage modulus (E') stabilises at around 9 MPa. The static property was calculated as 1.07 MPa at a normal strain of 0.05 using the published data. For the 55 Shore A sample the static modulus of elasticity was calculated as 0.975 MPa at the same strain. Using the ratio of static moduli and the measured storage modulus of the 60 Shore A sample the storage modulus was estimated as 8.2 MPa. Using the relationship found in equation 3.12 the shear storage modulus can be calculated and is 2.73 MPa.

3.4.2 Hollow cylinder

The first approximation is a plate of which the height and width are equal to the average height and circumference of a hollow cylinder. The average height of the plate is taken as half the sum of the inner surface height (l) and the outer surface height ($l + 2h_r$):

$$\bar{h} = l + h_r \tag{3.14}$$

The width of an equivalent plate is:

$$w = \pi\left(\frac{d_p + d_b}{2}\right) = \pi\bar{d} \tag{3.15}$$

The shear stiffness of the equivalent plate is therefore (Gere & Timoshenko, 1991):

$$k = \frac{GA}{t} = \frac{G\bar{h}\pi\bar{d}}{t} \tag{3.16}$$

where t is the spring thickness and is equal to ½(d_b - d_p). Equation 3.13 can only be applied to small strains. Summing the stiffness of rectangular flat sheets in series can approximate the spring shown in figure 3.9.

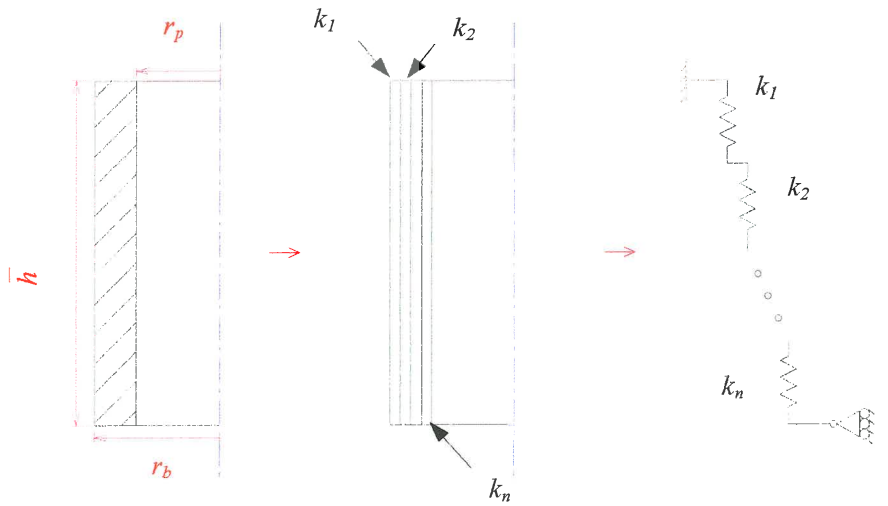

Figure 3.9 Approximation of the total spring stiffness

The total stiffness can be calculated by summation of the springs as shown in equation 3.17.

$$\frac{1}{k} = \sum_{i=1}^{n} \frac{1}{k_i} \tag{3.17}$$

k_i is defined by equation 3.16.

By substituting equation 3.16 and taking the sum of an infinite number of springs between r_p ($\frac{1}{2}d_p$) and r_b ($\frac{1}{2}d_b$) the following integral can be derived

$$\begin{aligned}\frac{1}{k} &= \int_{r_p}^{r_b} \frac{1}{2\pi G r \bar{h}} dr \\ &= \frac{1}{2\pi G \bar{h}} \int_{r_p}^{r_b} \frac{1}{r} dr \\ &= \frac{1}{2\pi G \bar{h}} \ln|r| \Big|_{r_p}^{r_b} \\ &= \frac{1}{2\pi G \bar{h}} [\ln(r_b) - \ln(r_p)]\end{aligned} \tag{3.18}$$

The stiffness for a hollow cylinder is therefore:

$$k = \frac{2\pi G \bar{h}}{\ln\left(\frac{r_b}{r_p}\right)} \tag{3.19}$$

The following formula takes the effect of combined bending and shear into account (Davey & Payne, 1964):

$$k = \frac{\bar{h} G}{\frac{1}{Q_1} + \frac{r_b^2}{\bar{h}^2 Q_2}} \tag{3.20}$$

Q_1 and Q_2 is defined as:

$$Q_1 = \frac{2\pi}{\ln\left(\frac{r_b}{r_p}\right)} \tag{3.21}$$

$$Q_2 = \frac{16\pi \left(\frac{r_b}{r_p}\right)^2 \left[\left(\frac{r_b}{r_p}\right)^2 - 1\right]}{3\left\{\left[\left(\frac{r_b}{r_p}\right)^2 - 1\right]^2 - 4\left(\frac{r_b}{r_p}\right)^2 \left[\ln\left(\frac{r_b}{r_p}\right)\right]^2\right\}} \tag{3.22}$$

Q_2 represents the bending and if this term is zero, the equation simplifies to equation 3.19.

The geometry was also analysed using finite elements. ABAQUS recommends that hybrid elements be used for an analysis involving incompressible materials. Higher order axi-symmetric elements gave the best results. The inner surface was displaced by 1 mm axially while any displacement normal to the surface was constrained. The outer surface was fully constrained. The reaction force on the outer surface was calculated by summation of all the constrained node reaction forces in the axial direction on this surface.

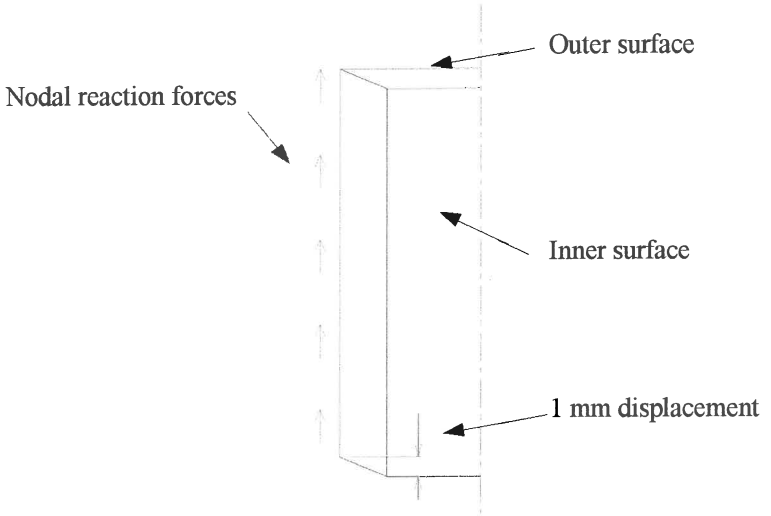

Figure 3.10 Schematic of the axi-symmetric finite element model (swept through 90°)

Several mesh refinements gave similar results and the best estimate is shown in table 3.12. Since the stiffness is a linear function of the shear modulus it will be more useful to report the results in terms of a stiffness coefficient. This coefficient can be used for any material, but only this specific geometry.

Table 3.12 Stiffness coefficients for a hollow cylinder

Method	Equation	Geometric stiffness (k/G)
Equivalent plate	3.16	2.592
Hollow cylinder	3.19	2.557
Hollow cylinder with bending	3.20	2.548
FEM estimate		2.492

3.4.3 Cylinder with tapered ends

If the tapered ends of the cylinder are taken into account the following equation should be used (Davey & Payne, 1964):

$$k = \frac{2\pi G\left[(l+2h_r)r_p - lr_b\right]}{(r_b - r_p)\left[\ln\left((l+2h_r)r_p\right) - \ln(lr_b)\right]} \qquad (3.23)$$

This equation is compared to the finite element model of a spring with tapered ends in table 3.13.

Table 3.13 Tapered cylinder results

Method	Equation	Geometric stiffness (k/G)
Tapered hollow cylinder	3.23	2.534
FE estimate		2.522

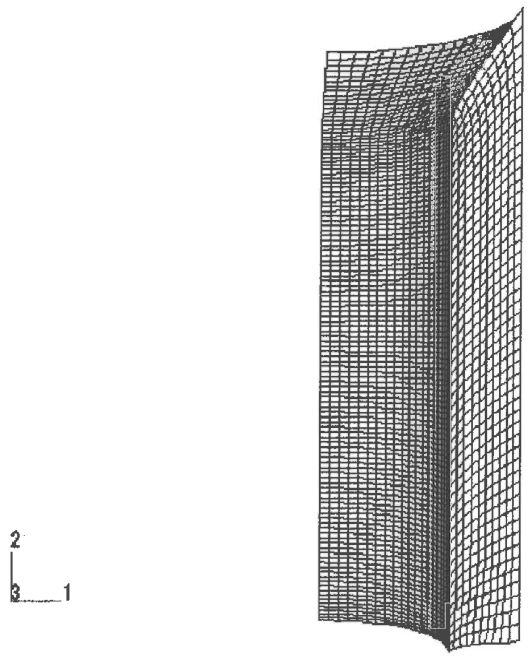

Figure 3.11 Exaggerated deformation and mesh of the spring with tapered ends (swept through 90°)

The results show that the average height and circumference assumption slightly overestimated the spring stiffness. The finite element model showed no mesh size or element type dependency.

3.4.4 Exact geometry

The previous analysis showed that the tapered ends do not have a large effect on the stiffness. It might therefore be possible to ignore their effect during the design especially if the ratio between the port length and reservoir height is large. The side entrances will, however, have a major impact due to its size. The spring can theoretically be divided into four springs that act in parallel as shown in figure 3.12.

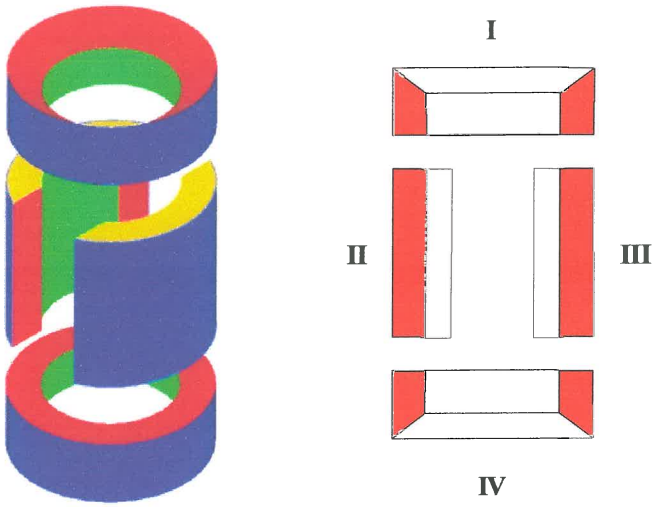

Figure 3.12 Subdivision of the absorber spring

The springs will be numbered from I to IV. It is obvious from the symmetry of the model that the stiffness of spring I and II is equal to that of spring III and IV. The total stiffness is therefore:

$$k = 2(k_I + k_{II}) \tag{3.24}$$

The section dimensions of spring I are shown in figure 3.13.

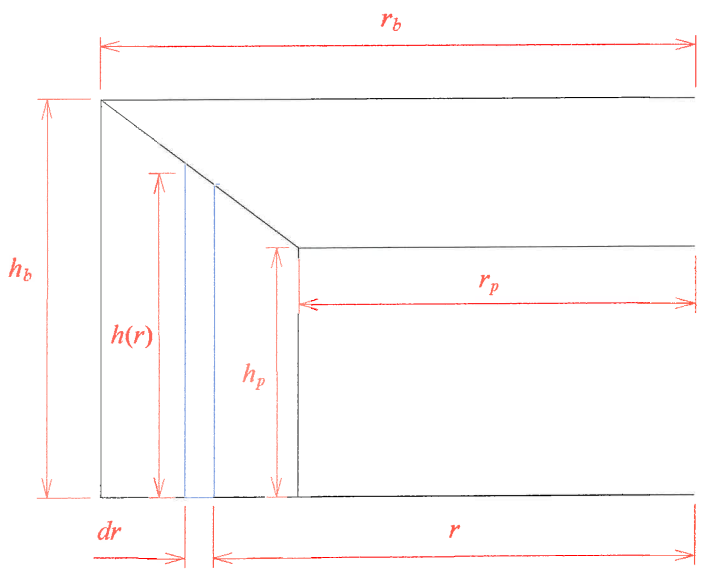

Figure 3.13 Section dimensions for spring I

The total stiffness of the shape in figure 3.13 can be found through the summation of rectangular sheets of infinitesimal thickness according to the rule for summation of springs in series. The height of the sheet is a function of the radius and is given by equation 3.25:

$$h(r) = \frac{r - r_p}{r_b - r_p}\left(h_b - h_p\right) + h_p \tag{3.25}$$

The width of the sheet is $2\pi r$. The stiffness of the sheet is given by equation 3.26:

$$dk = \frac{GA}{dr} = \frac{2\pi Gr\left[\frac{r - r_p}{r_b - r_p}\left(h_b - h_p\right) + h_p\right]}{dr} \tag{3.26}$$

The inverse of the stiffness of spring I can now be calculated by evaluating the following integral:

$$\frac{1}{k_I} = \int_{r_r}^{r_b} \frac{1}{2\pi Gr\left[\frac{r - r_p}{r_b - r_p}\left(h_b - h_p\right) + h_p\right]} dr \tag{3.27}$$

This integral will be evaluated numerically.

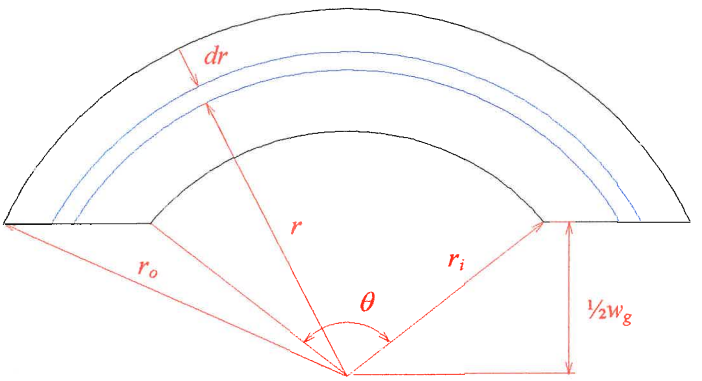

Figure 3.14 Section dimensions of spring II

The spring has height h_g. The inverse of the stiffness is:

$$\frac{1}{k_{II}} = \int_{r_r}^{r_b} \frac{dr}{2Grh_g \operatorname{acos}\left(\frac{w_g}{2r}\right)} = \frac{1}{2Gh_g}\int_{r_r}^{r_b} \frac{1}{r \operatorname{acos}\left(\frac{w_g}{2r}\right)} dr \tag{3.28}$$

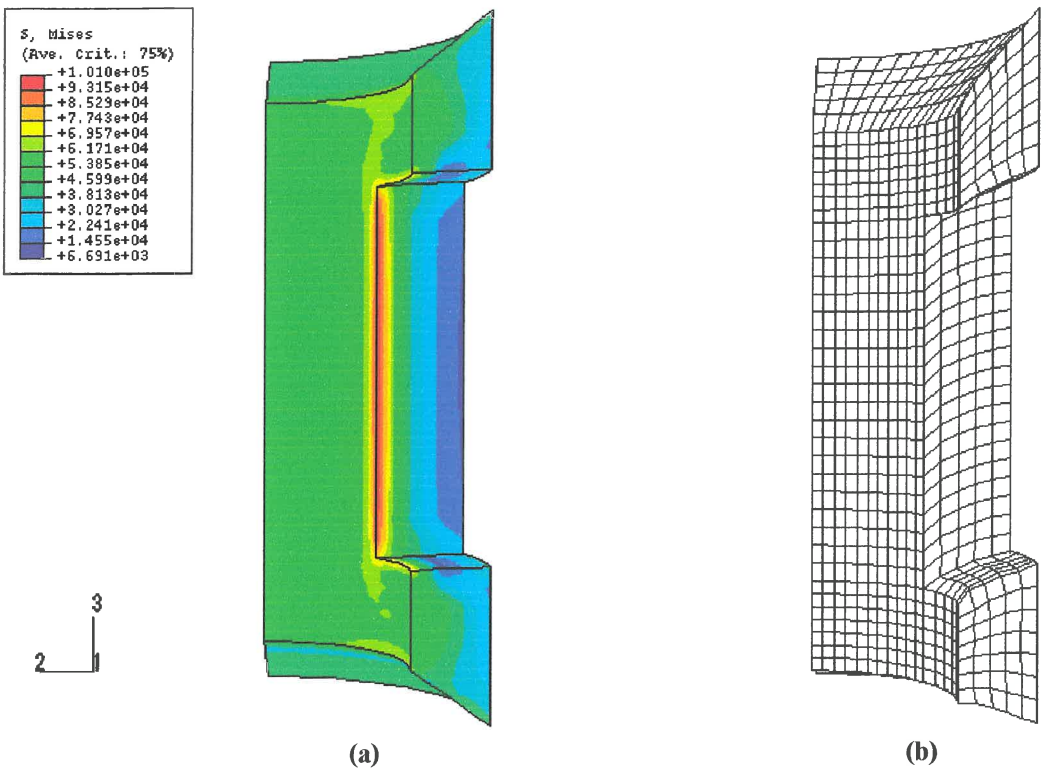

Figure 3.15 (a) Von Mises stress contours and (b) exaggerated deformation for a ¼ section of the absorber spring

For the finite element approximation 3D brick elements were used. In this case it was possible to simplify the analysis by only modelling ¼ of the absorber spring. Various element types and mesh sizes gave similar results. The von Mises stress contours show that care should be taken with the entrance design to ensure minimal stress concentration.

The results of the finite element model estimate and the integration of the geometry are shown in table 3.14. As expected the side entrances have a major effect on the resulting geometric stiffness if compared to the result in table 3.13. The exact geometry integration is very close to the finite element result and it is therefore recommended that this method be used for the calculation of the spring stiffness for design purposes.

Table 3.14 Exact geometry

Method	Equation	Geometric stiffness (k/G)
Exact geometry integration	3.24	1.985
FE estimate		1.921

For the estimate of the shear modulus made in §3.4.1 (2.37 MPa) the spring stiffness will be 4.55 MN/m which is close enough to the assumed value of 4 MN/m.

3.4.5 Casting of the polyurethane spring

The elastomeric spring was cast by fitting polypropylene moulds on the ends of the sleeve and in the side entrances as shown in figure 3.16. All the areas where the polyurethane should stick to the surface were treated with an adhesive. The rest of the port, sleeve and moulds were treated with a release agent. The moulds also had to ensure the proper alignment of the port and the sleeve. This was achieved by machining a locating pin on the ends of the plug moulds. The entrance moulds were screwed onto the port to ensure that the port does not rotate about its centre axis. This alignment is important to ensure that the centrelines of the two load cell connection points coincide. The moulds also prevented the polyurethane from leaking into the port during casting. The entrance moulds were machined slightly smaller than the entrances. The resulting gap was filled with putty. A riser was machined into the top mould to accommodate the shrinkage that occurs as a result of polymerisation.

The polyurethane was supplied as a three component casting system consisting of resin base, isocyanate and 1,4-butane diol. These three compounds are mixed in a specific ratio that will determine its mechanical properties. The mixture is castable for ±15 min. During this time it is important to limit the formation of bubbles, which will become inclusions in the spring after it is cast. Centrifugal force is used to drive the bubbles to the surface of the mixture.

The mould assembly was evenly heated to about 40°C in an oven to accelerate the chemical reaction. After it has been cast the top entrance mould was bolted in place to ensure that all the polyurethane was driven from the interface with the port. The spring cured within 2 days.

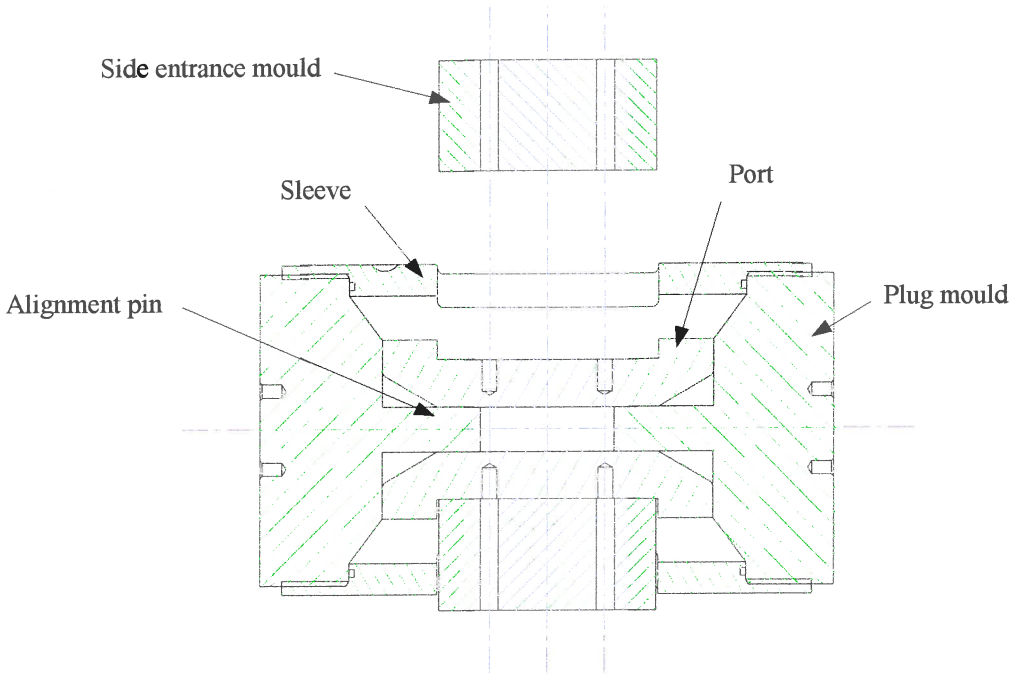

Figure 3.16 Mould assembly for the casting of the polyurethane spring

3.5 Calculation of the viscous damping

The viscous damping is calculated as described in chapter 2. For this design the geometry differs from the theoretical case and this will affect the damping significantly. Since the method was explained in detail in chapter 2 this paragraph will focus on the improvement obtained with the use of the new geometry. Appendix E contains more detailed results from this analysis as well as description of the methods used. The mesh is shown in figure 3.17.

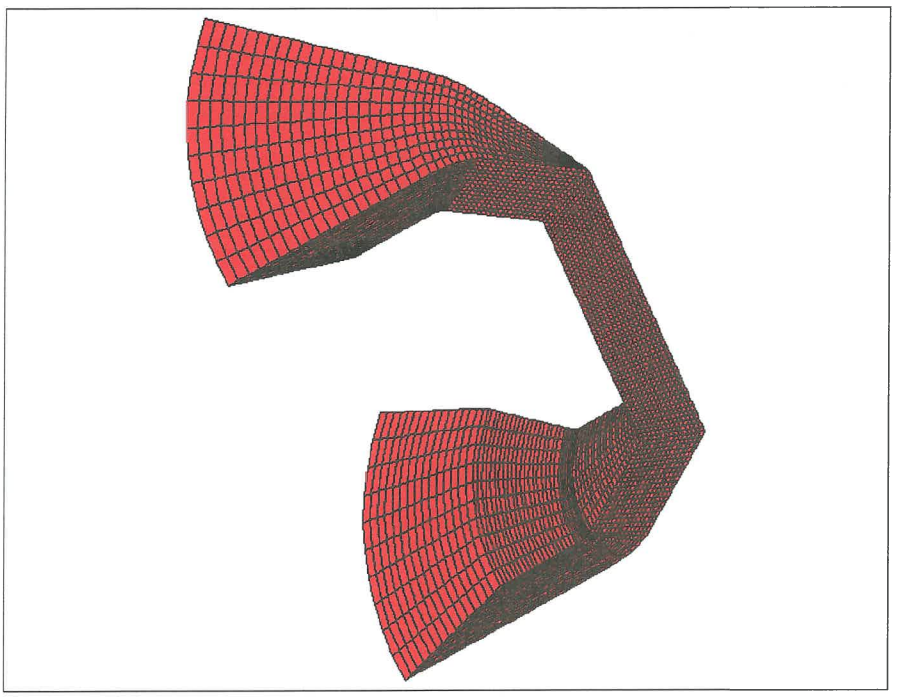

Figure 3.17 3D grid for 1/8th of the flow region

A comparison between the results for a square and a conical inlet/outlet at a port velocity of 0.2 m/s is shown in table 3.15.

Table 3.15 Comparison at a port velocity of 0.2 m/s

	Theoretical value / Design value
Inlet pressure drop	4.5
Outlet pressure drop	1.9
Total pressure drop	2.7
Viscous damping	5.1

The inlet pressure drop was the main contributor to the 5.1 times reduction in viscous damping. This is a significant improvement and it can probably be reduced further using optimisation techniques. However, an optimised port inlet/outlet might be expensive to manufacture.

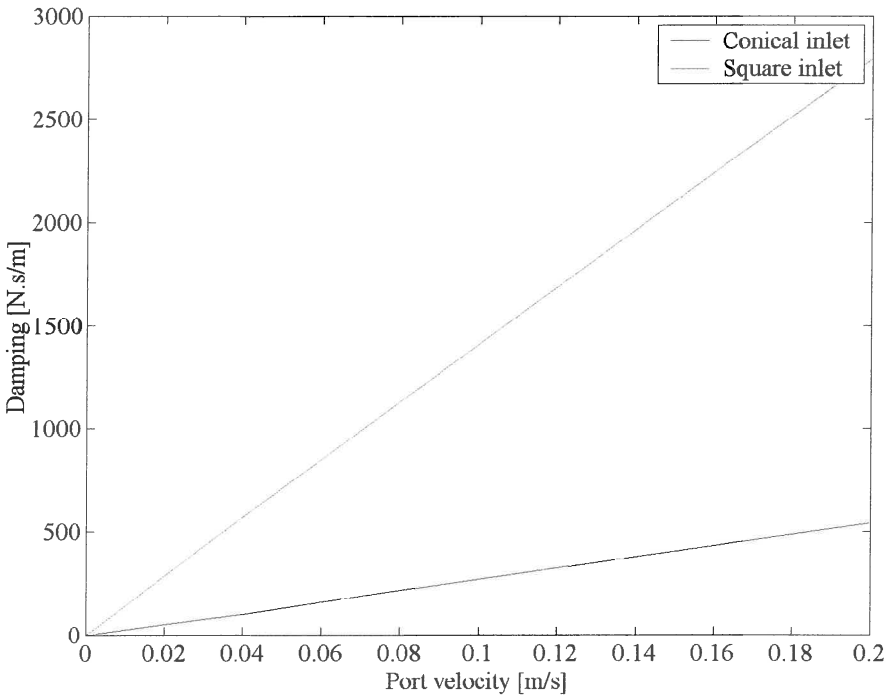

Figure 3.18 Viscous damping (c) as a function of port velocity ($\dot{x}$)

3.6 Conclusion

It is possible to find the optimal geometry of a damped LIVE type absorber for a desired frequency of isolation taking into account the various practical requirements. The port length must be adjusted to account for the addition of conical inlets/outlets. The spring stiffness should be calculated to ensure that it is viable with the chosen elastomeric material. If this proves impossible the outer port diameter can be modified. The port inlet/outlet geometry must be optimised to ensure the lowest possible viscous damping.